Fermi-surface mapping from Compton profiles: Application to beryllium

G. Kontrym-Sznajd and M. Samsel-Czekała
W. Trzebiatowski Institute of Low Temperature and Structure Research, Polish Academy of Sciences, P.O. Box 1410, 50-950 Wrocław 2, Poland

S. Huotari, K. Hämäläinen, and S. Manninen
Division of X-ray Physics, Department of Physical Sciences, P.O. Box 64, FIN-00014 University of Helsinki, Finland
(Received 9 June 2003; revised manuscript received 1 August 2003; published 9 October 2003)

The two-dimensional momentum density of Be on the basal ΓMK plane, i.e., the line integral of the three-dimensional momentum density along the *c* axis, is reconstructed via the Cormack method from both experimental and theoretical Compton profiles. It is shown that in the case of Be, despite the momentum density being highly anisotropic, merely two Compton profiles are sufficient to reproduce the main features of the momentum density. The analysis of the reconstructed densities is performed both in the extended and reduced zone schemes.

DOI: 10.1103/PhysRevB.68.155106 PACS number(s): 71.18.+y, 13.60.Fz, 87.59.Fm

I. INTRODUCTION

During the last few decades, Compton scattering has been widely used as a probe of the electronic structure of matter. Within certain approximations,[1] the experimental double-differential inelastic x-ray scattering cross section can be related to the Compton profile, which is a double (plane) integral of the electron density in the extended momentum space, $\rho(\mathbf{p})$,

$$J(p_z)=\int_{-\infty}^{\infty}\rho(\mathbf{p})dp_x dp_y. \tag{1}$$

The Compton profile, being related directly to occupied electronic ground states, contains information not only on the Fermi surface (FS) but also on the umklapp components of the electron wave functions.

Equation (1) represents the Radon transform[2] of $\rho(\mathbf{p})$ in three-dimensional (3D) space over 2D hyperplanes. The first reconstruction method based on the inversion of the Radon transform was Mijnarends's method.[3] Other alternative solutions are Fourier transform algorithms,[4,5] the maximum entropy technique,[6] and two different methods employing orthogonal polynomials.[7,8]

In cases where the electron momentum density is a strongly anisotropic function, reconstruction of the 3D momentum density from 1D Compton profiles is rather elaborate, since a large number of measurements is needed. Thus a reconstruction of 2D momentum densities from Compton profiles[9] is proposed, i.e., a conversion from double (plane) integrals in Eq. (1) to a single (line) integral of the form

$$\rho^{\mathbf{L}}(p_z,p_y)\equiv J(p_z,p_y)=\int_{-\infty}^{\infty}\rho(\mathbf{p})dp_x, \tag{2}$$

where $\mathbf{L}||p_x$. When studying the structure of the Fermi surface, this 2D momentum density can be interpreted much more easily than the Compton profiles. Furthermore, it can be directly compared to corresponding 2D angular correlation of positron annihilation radiation (ACAR) results, yielding additional information on the electron-positron interaction. It is also much easier to reconstruct accurately than the 3D momentum density $\rho(\mathbf{p})$ because the number of required Compton profiles is relatively small. 2D momentum densities can also be folded into the first Brillouin zone (BZ) in order to delineate various FS elements.

This procedure is demonstrated for beryllium metal by using two Compton profiles, taken with the p_z axis along the reciprocal lattice vectors [100] and [110]. In this case the 2D momentum density can be reconstructed with the integration axis along [001]. The resulting densities are shown both in the extended and reduced zone schemes. For obtaining the density in the reduced zone scheme, the Lock-Crisp-West (LCW) procedure[10] is used.

II. CONVERSION FROM 1D TO 2D SPECTRA

The purpose of this work is to reconstruct $\rho^{\mathbf{L}}(p_z,p_y)$, with $\mathbf{L}||[001]$, from its line integrals, i.e., from the Compton profiles

$$J(p_z)=\int_{-\infty}^{\infty}\rho^{\mathbf{L}}(p_z,p_y)dp_y. \tag{3}$$

For this, the Cormack method[11] is proposed, corresponding to the solution of the Radon transform in 2D space over 1D hyperplanes.

If the direction p_x is along an *R*-fold rotation axis of the lattice, both the Compton profiles and the 2D momentum density can be expanded into a cosine series

$$\rho^{\mathbf{L}}(p_z,p_y)\equiv\rho(p,\Theta)=\sum_{i=0}^{\infty}\rho_{iR}^{\mathbf{L}}(p)\cos(iR\Theta), \tag{4}$$

$$J(p_z)\equiv J(t,\varphi)=\sum_{i=0}^{\infty}g_{iR}(t)\cos(iR\varphi). \tag{5}$$

Here (t,φ), where $t=|p_z|$, are the polar coordinates of p_z in the laboratory coordinate system, while (p,Θ) are the polar coordinates of the momentum (p_z,p_y) in the crystal coordinate system.

By applying the Cormack method,[11] $\rho^{\mathbf{L}}(p_z,p_y)$ can be evaluated from Eq. (4) where its radial components $\rho_l^{\mathbf{L}}(p)$ for $l=iR$ are given by

$$\rho_l^{\mathbf{L}}(p)=\sum_{k=0}^{\infty}(l+2k+1)a_{lk}R_l^k(p). \tag{6}$$

$R_l^k(p)$ are the Zernike polynomials and the coefficients a_{lk} are obtained from the series expansion of $g_l(t)$,

$$g_l(t)=2\sum_{k=0}^{\infty}a_{lk}\sqrt{1-t^2}U_{l+2k}(t), \tag{7}$$

where $U_m(t)$ are the Chebyshev polynomials of the second kind. Since they are orthogonal in $[-1,1]$,

$$a_{lk}=\frac{1}{\pi}\int_{-1}^{1}g_l(t)U_{l+2k}(t)dt. \tag{8}$$

To use the symmetry properties most profitably, the best choice is to measure $J(p_z)$ for p_z perpendicular to the [001] direction. The directions of p_z [Eq. (5)] should be equally spaced in the nonequivalent part of the BZ, which ranges in the ΓMK plane from $\varphi=0°$ up to 45° (or 30°) for cubic and tetragonal (or hexagonal) structures, respectively. If N projections are to be measured for the structure with an R-fold rotation axis along the [001] direction, the best orientation of the nth projection $(n=1,2,\ldots,N)$ is given by the formula $\varphi_n=\Delta\varphi/2+(n-1)\Delta\varphi$ where $\Delta\varphi=\pi/(RN)$. However, if for any particular reason one would like to perform measurements also for the main symmetry directions, the orientation of the nth projection ought to be determined from the formula $\varphi_n=(n-1)\Delta\varphi'$ where $\Delta\varphi'=\pi/[R(N-1)]$.

In this way one can estimate $J(p_z,p_y)$, which represents the line integral of the density along the [001] direction. This procedure has already been applied to 1D ACAR spectra of yttrium.[9] Even though the momentum density of Y is highly anisotropic, only three projections were needed to obtain almost all details of the 2D momentum density. In this work, the method is successfully applied to beryllium (another hcp metal) in the extreme case of merely two measured projections available.

III. APPLICATION TO BERYLLIUM DATA

The Be Compton profiles were measured at the European Synchrotron Radiation Facility (ESRF) beam line ID15B using 29 keV photons. The details of the experiment are described in Ref. 12. Two projections were measured with p_z along ΓM and ΓK and with an overall momentum resolution of 0.1 a.u. The corresponding highly accurate theoretical profiles were calculated with the Korringa-Kohn-Rostoker (KKR) local-density approximation (LDA) method.[13] Such spectra allow the reconstruction of $\rho^{\mathbf{L}}\equiv J(p_z,p_y)$ with p_x along the hexagonal c axis. This 2D momentum density will be denoted as $\rho^{001}(p_z,p_y)$.

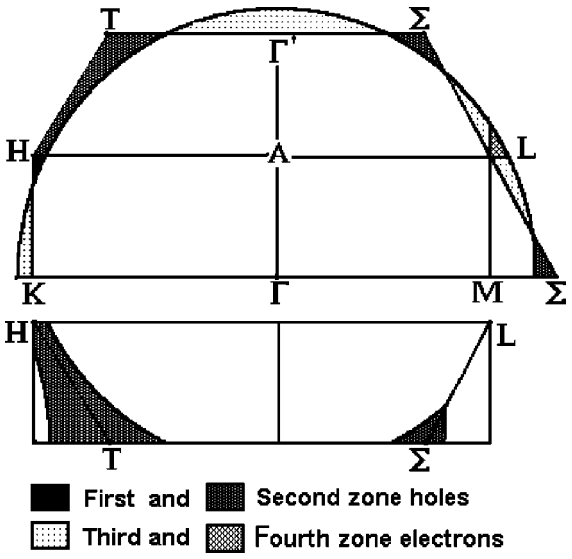

FIG. 1. Free-electron Fermi surface of Be in the ΓAK and ΓAM planes in the extended (upper panel) and reduced zone scheme (lower panel).

Let us choose the polar system (p_y',p_z'), fixed to the lattice, with p_z' along the ΓK direction. The measured profiles, $J(p_z)\equiv J(t,\varphi)$, are described by the polar angle $\varphi=0°$ for p_z along ΓK and $\varphi=30°$ for p_z along ΓM. In this case two radial functions $g_l(t)$ with $l=0$ and 6 can be determined from Eq. (5),

$$\begin{aligned} g_0(t)&=[J_{\Gamma K}(t)+J_{\Gamma M}(t)]/2,\\ g_6(t)&=[J_{\Gamma K}(t)-J_{\Gamma M}(t)]/2. \end{aligned} \tag{9}$$

It is convenient to choose the unit system so that $t'=t/t_{max}=\cos(\alpha_i)$. The zeros of the Chebyshev polynomials $U_m(t')$ occur then at $\alpha_i=(\pi/2m)(2i+1)$ with $i=0,1,\ldots,m-1$, and

$$a_{lk}=\frac{1}{M}\left\{\sum_{i=1}^{M-1}g_l[\cos(i\Delta\alpha)]\sin[(2k+l+1)i\Delta\alpha]+\frac{1}{2}(-1)^{k+l/2}g_l(0)\right\}, \tag{10}$$

where $\Delta\alpha=\pi/2M$, and M is the number of points used in the evaluation of a_{lk}. In this work, $M=720$ $(\Delta\alpha=0.125°)$, which allows one to calculate 150 coefficients a_{lk} for each $g_l(t)$. This is equivalent to applying the Gaussian quadratures for the polynomials up to the 300th order.

The FS of Be for the free-electron model is presented in Figs. 1 and 2. To the authors' knowledge, the first realistic band-structure calculations for Be were performed with the orthogonalized plane-wave (OPW) method.[14] The results of that study, compared to the free-electron model, suggested the following FS features: (a) no holes around the H point either in the first or second band (first zone fully occupied and no holes in the second zone on the plane AHL); (b) very

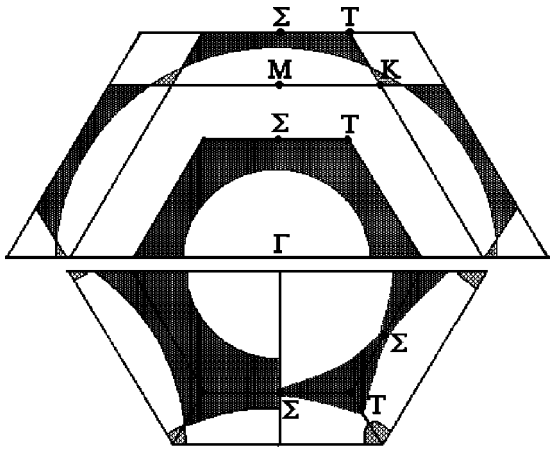

FIG. 2. The Fermi surface of Be in the ΓMK plane. Upper panel: Free-electron model in the extended zone scheme. Lower left panel: Free-electron model in the reduced zone scheme. Lower right panel: Real FS derived from Ref. 14.

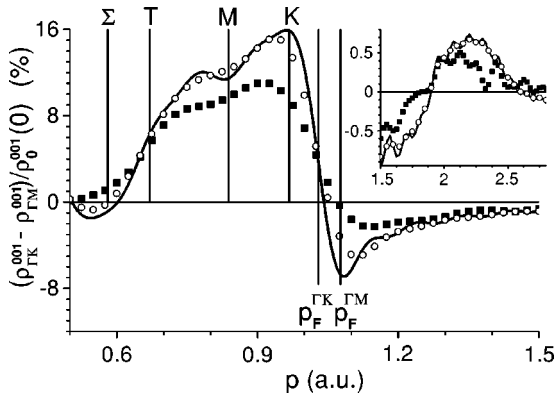

FIG. 3. Differences between 2D densities of Be for momenta along ΓK and ΓM, reconstructed from two Compton profiles. The experimental results are indicated by solid squares. The corresponding results of the reconstruction from theoretical Compton profiles with and without resolution broadening are shown by open circles and solid line, respectively.

small holes around Σ and reduced holes around T in the second zone when compared to the free-electron model; (c) no electrons around Γ in the third band; (d) no electrons around L either in the third or fourth bands; and (e) cigars in the third zone around K are larger than for the free-electron model with their height close to $|KH|$ (see Fig. 2). These results were supported by de Haas–van Alphen (dHvA) experiment[15] with two main differences: the computational cigars were triangular and the coronet was slightly larger than observed by the dHvA experiment.

Further theoretical band structure results[16,17] were similar to those in Ref. 14 while the latest linear combination of atomic orbital (LCAO) results[18] turned out to be somewhat different, i.e., Fig. 3 in Ref. 18 representing $\rho(\mathbf{p})$ along $[011] \equiv \Gamma L$ points out that there are electrons around the L point in the third and fourth bands. Theoretical Compton spectra used in this work[13] agree qualitatively with the band-structure results in Ref. 14.

The results in the extended zone scheme along two main symmetry directions ΓK and ΓM are displayed in Figs. 3 and 4. Figure 3 presents the anisotropy of the 2D momentum density $\rho^{001}(\mathbf{p})$ for $\mathbf{p} \| \Gamma K$ and $\mathbf{p} \| \Gamma M$, reconstructed from both the experimental and theoretical Compton profiles taken from Refs. 12 and 13. The widely used approximation to include the electron-electron (e-e) correlation into the momentum densities is the so-called Lam-Platzman (LP) correction.[19] However, this correction is isotropic and thus does not have any effect on the anisotropy of theoretical curves in Fig. 3. The resolution function of the experimental apparatus smears some of the fine structure of the data as indicated in the figure.

For momenta $0.60 < p < 1.05$ a.u. (atomic units of momentum), the reconstructed 2D densities have much larger values for $\mathbf{p} \| \Gamma K$ than for $\mathbf{p} \| \Gamma M$. This is due to the fact that for the real FS there are no electrons in the third or fourth bands around the L point. This is seen in Fig. 3 as a positive anisotropy. The largest positive values for $|\Gamma M| \leqslant p \leqslant |\Gamma K|$ are, additionally, a manifestation of the lack of holes around the H point. The negative anisotropy for $p > 1.05$ a.u., with the minimum at $p = p_F^{\Gamma M}$, originates from the fact that $p_F^{\Gamma M} > p_F^{\Gamma K}$, i.e., the holes around the Σ point, shown in the lower panel in Fig. 2, are very small. Umklapp components for $p > 1.9$ a.u. along ΓK are also observed. These results are in good agreement with the theoretical 3D momentum density[13] and the experimental observation of the umklapp components.[20] All subtle features of the theoretical anisotropy are reproduced by the experiment in detail. The accuracy of this result is due to the fact that even with three Compton profiles available (the third one measured with $\varphi = 15°$), the function $g_6(t)$ and thus also $\rho_6^{001}(p)$ as well as the anisotropy, $\rho_{\Gamma K}^{001}(p) - \rho_{\Gamma M}^{001}(p) = 2\rho_6^{001}(p)$, would be the same as obtained from two projections.[21] The fact that the magnitude of the anisotropy (''seen'' in the experiment) is diminished indicates that e-e correlation has an anisotropic effect on the momentum density, as has been suggested earlier.[12]

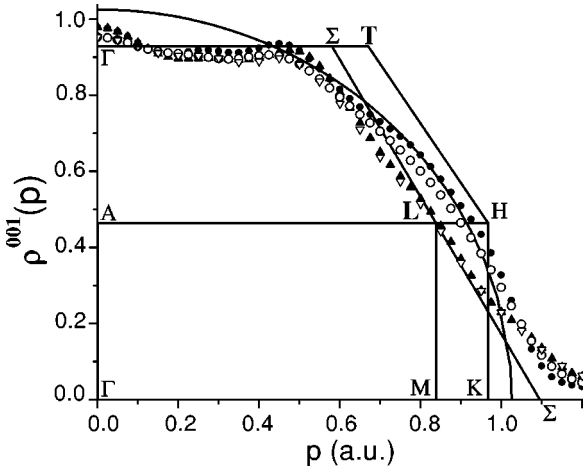

FIG. 4. 2D momentum densities of Be, normalized to dimensions of the BZ's, for momenta along ΓK (circles) and ΓM (triangles), reconstructed from two Compton profiles. Theory (including resolution broadening and the Lam-Platzman correction) and experiment are marked by solid and open symbols, respectively.

Reconstructed densities for momenta along ΓK and ΓM are presented in Fig. 4. It can be seen that the absolute densities are not reproduced exactly, e.g., a small electronlike lens is observed at $p=0$ a.u. According to all previous band-structure calculations, this element should not be present and is thus most probably an artifact originating from the fact that the isotropic component $\rho_0^{001}(p)$ is reconstructed from only two projections. However, this artifact is cancelled out in the difference shown in Fig. 3, which further demonstrates the accuracy of the obtained anisotropy.

Concerning the influence of statistical noise on the reconstructed densities, $\sigma[\rho^{001}(\mathbf{p})]$, we performed the following tests. (1) The quality of data was checked by the consistency condition (CC).[22] According to the CC, three first coefficients of the expansion of spectra $J_{\Gamma K}(p)$ and $J_{\Gamma M}(p)$ into orthogonal polynomials must be exactly the same. The experimental Be Compton profiles used in this work satisfied this condition perfectly, indicating both high statistical and systematic accuracy of the data. (2) By performing simulations of noise, added to theoretical profiles (similarly as in Ref. 22) we obtained that, due to the very good experimental accuracy and the relatively small core contribution, $\sigma[\rho^{001}(\mathbf{p})]<0.15\%$ in units of $\rho^{001}(\mathbf{p=0})$, which is equivalent to 6% of the maximum of theoretical anisotropy $\rho_{\Gamma K}^{001}(p)-\rho_{\Gamma M}^{001}(p)$. However, such an error occurs for low momenta (<0.6 a.u.), not shown in Fig. 2. (3) By applying in the reconstruction orthogonal polynomials that have mean-square approximation properties, we were able to gain some control on which fluctuations of the reconstructed densities could be connected with statistical noise, and to remove this noise to some extend.

Moreover, the highest statistical error occur along the high symmetry directions because of extreme values of the lattice harmonics [in our case $cos(6\varphi)$] along ΓK and ΓM. This follows from the fact that spectra were measured only in the nonequivalent part of the Brillouin zone. Thus, data (therefore also the noise) are expanded into lattice harmonics, which means that spectra for equivalent directions must be the same. In this way the symmetry condition was imposed also on the noise. However, such an error is smaller than the truncation error, following from the limited number (in our case to 2) of projections used in the reconstruction and does not influence the obtained results, the more so as we restrict our analysis to drawing the qualitative FS.

In the analysis in the **p** space one should bear in mind that $\rho^{001}(p_z,p_y)$ cannot be directly identified with the FS line dimensions along the [001] direction because in real metals $\rho_j(\mathbf{p})$ (in jth band) is lower than 1 even in the central FS. However, undoubtedly the theoretical as well as the experimental results show the lack of electrons around the L point in the third and fourth bands and the shape of the FS on the ΓMA plane close to the double BZ boundaries. In order to obtain more detailed information, $\rho^{001}(p_z,p_y)$ has to be folded to the reduced zone scheme (**k** space) as discussed in the following.

IV. RESULTS OF THE LCW FOLDING PROCEDURE

In the Compton-scattering experiment one measures the electron density in the **p** space

$$\rho(\mathbf{p}=\mathbf{k}+\mathbf{G})=\sum_j^{occ}\left|\int_{-\infty}^{\infty}\phi_{\mathbf{k}j}(\mathbf{r})e^{-i\mathbf{p}\cdot\mathbf{r}}d\mathbf{r}\right|^2, \tag{11}$$

where **k**, **G**, j, and $\phi_{\mathbf{k}j}(\mathbf{r})$ denote the wave vector, reciprocal lattice vector, band index, and electron wave function in the state $\mathbf{k}j$, respectively. The summation is over all occupied states. In a periodic lattice potential, the momentum density in the jth band can be written as

$$\rho_j(\mathbf{k}+\mathbf{G})=n(\mathbf{k}j)\ \ |u_{\mathbf{k}j}(\mathbf{G})|^2, \tag{12}$$

where $u_{\mathbf{k}j}$ are the Fourier coefficients of the electron wave functions and $n(\mathbf{k}j)$ is the occupation number.

It is well known that it is not possible to obtain the shape of the FS knowing only the density $\rho(\mathbf{p})$. This is due to the fact that the density is not constant on the FS and $\rho(\mathbf{p})$ represents a sum of contributions from all occupied bands, not only those crossing the Fermi energy. Thus, in order to obtain the FS map, the best choice is to perform LCW folding,[10] which is a conversion from **p** to **k** space. By doing this, the folded densities visualize the shape of the individual FS elements more clearly.

In the case of the electron density (neglecting correlation effects), $\rho_j^e(\mathbf{k})=\Sigma_{\mathbf{G}}\rho_j^e(\mathbf{k}+\mathbf{G})=n(\mathbf{k}j)=1$ (or 0 for unoccupied states) and $\rho^e(\mathbf{k})=\Sigma_j\rho_j^e(\mathbf{k})=n(\mathbf{k})$, where n denotes the number of occupied bands contributing to the point **k**. The application of the LCW folding to $\rho^{\mathbf{L}}(p_z,p_y)$ gives the function $\rho^{\mathbf{L}}(k_z,k_y)$ which represents the corresponding line integral of $\rho(\mathbf{k})$, in this case along $\mathbf{L}\|[001]$. The density $\rho^{\mathbf{L}}(k_z,k_y)$ can be identified with the sum of the FS line dimensions over occupied bands along **L**.

The results of the folding procedure are displayed in Fig. 5, where densities $\rho^{001}(k_z,k_y)$ reconstructed from two theoretical and two experimental Compton profiles, are presented. The free-electron model result is also shown for comparison.

Conventionally, the momentum densities $\rho(\mathbf{k})$ obtained via the LCW folding, and thus also densities $\rho^{001}(k_z,k_y)$, are presented in arbitrary scale. As was shown by Kaiser *et al.*,[23] the main reason is that the convergence of the LCW procedure is dependent on the degree of the localization of the electrons. The more localized they are, the larger the contribution of the umklapp components at high momenta is, which consequently increases the truncation error of the LCW procedure. This effect decreases the LCW-folded densities in a nonuniform way, and thus an absolute normalization is difficult. In the case of experimental densities, the finite resolution function and statistical noise, both affecting especially the umklapp components, complicate the normalization even further.

In Be the volume of occupied valence states is equal to the volume of two BZ's. Thus, if two bands were completely filled, $\rho^{001}(k_z,k_y)$ would be constant and equal to $2|\Gamma A|$. The light and dark areas in Fig. 5 depict low and high electron densities originated from the holes in the second band (coronet) and the electrons around K in the third band (cigars), respectively.

Figure 6 shows the same densities in more detail along the main symmetry directions together with densities obtained

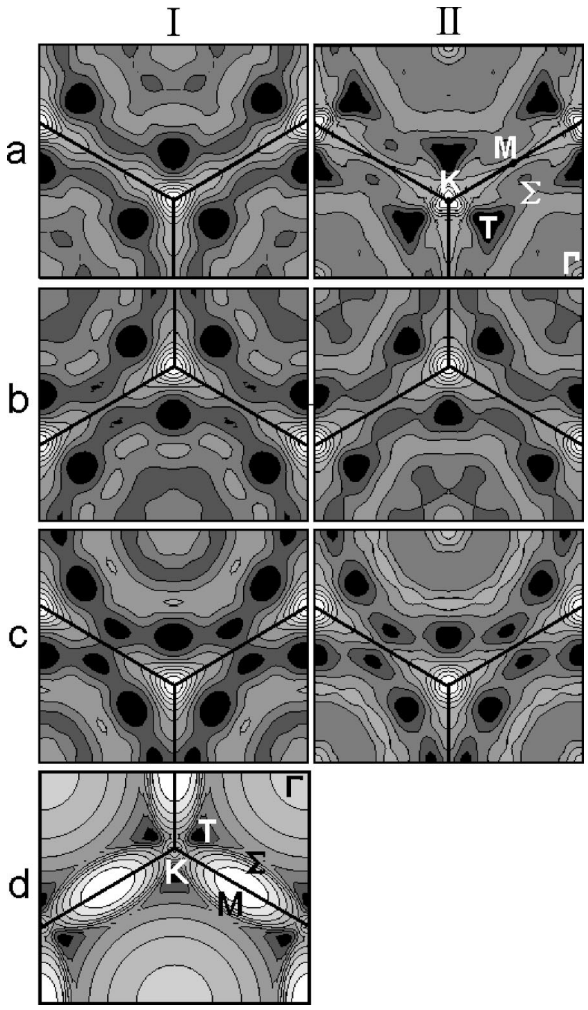

FIG. 5. 2D LCW densities $\rho^{001}(k_z,k_y)$ in Be, in the repeated zone scheme, reconstructed from two 1D projections. Panel (a): Theory without LP correction. Panel (b): Theory with LP correction and resolution broadening. Panel (c): Experiment. Panel (d): Free-electron model. Columns I and II show results described by 60 and 90 [or 120 in panel (a)] orthogonal polynomials, respectively. Each figure contains 10 contour lines.

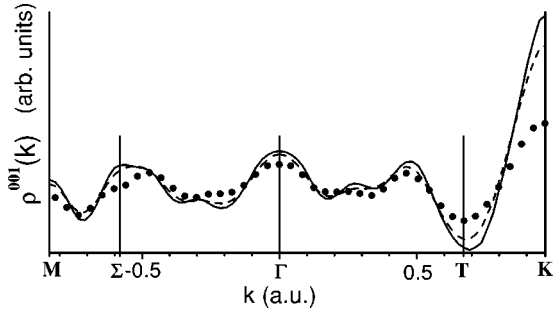

FIG. 6. 2D LCW densities in Be for momenta along ΓK (right-hand side) and ΓM (left-hand side), reconstructed from two 1D spectra. The theory with LP correction with and without resolution broadening is indicated by dashed and solid lines, respectively, while the experiment is marked by circles.

from the corresponding LP-corrected theoretical Compton profiles. From Figs. 5 and 6 the second-zone holes around T and the third-zone electrons around K can be clearly recognized. Other features, e.g., the electronlike artifact around the Γ point in the third band (seen also in Fig. 4) and a holelike artifact between the Σ and M points, are caused by using only two components of reconstructed density $\rho^{001}(p_z,p_y)$, determined from only two Compton profiles.

V. SUMMARY

When the electron momentum density $\rho(\mathbf{p})$ is highly anisotropic, it is quite difficult to obtain its shape from 1D projections accurately, since a relatively large number of projections is needed. For these cases, the reconstruction of 2D momentum densities $J(p_z,p_y)$ instead of 3D densities $\rho(\mathbf{p})$ is advised. It is shown that only a small number (2–5) of measured plane projections is needed to reconstruct the 2D momentum density, and generally this 2D density allows much more detailed analysis of the FS than 1D projections. The use of the Cormack method is proposed, because (a) the expansion of measured spectra into orthogonal polynomials has mean-squares approximation properties and thus it effectively smooths the statistical noise in the experimental data;[24] (b) the method employs the Chebyshev polynomials, which are the only orthogonal polynomials having analytical zeros, allowing the estimation of the coefficients a_{lk} to a high degree of precision.

This method was applied to two Be Compton profiles and the line projection of the momentum density along the [001] direction was reconstructed. The analysis performed in the extended **p** space shows that for $0.60<p<1.05$ a.u. the line dimensions of the FS along [001] are much larger for $\mathbf{p}\|\Gamma K$ than for $\mathbf{p}\|\Gamma M$, which is caused by the lack of electrons in the third and fourth bands around the L point and the lack of holes around the H point. The anisotropy of the Fermi momentum, i.e., $p_F^{\Gamma M}>p_F^{\Gamma K}$, leading to very small holes around the Σ point, is also observed. All subtle features of the theoretical anisotropy are reproduced by the experiment in detail. However, its magnitude is diminished, which indicates that e-e correlation has an anisotropic effect on the momentum density. With the example of the anisotropy $\rho_{\Gamma K}^{001}(p)-\rho_{\Gamma M}^{001}(p)$, it is shown how symmetry properties can enhance the accuracy of the reconstruction.

After folding the reconstructed densities $\rho^{001}(p_z,p_y)$ into the reduced zone scheme, the second zone holes and third zone electrons could be clearly recognized around the T and K points, respectively. Moreover, the results both in **p** and **k** spaces clearly show the absence of the FS elements around the L point in the third and fourth bands.

ACKNOWLEDGMENTS

The authors are grateful to S. Kaprzyk and A. Bansil for making the theoretical Compton profiles of Be available. The European Synchrotron Radiation Facility is acknowledged for the provision of synchrotron radiation facilities and the authors would like to thank Dr. Thomas Buslaps for assistance in using beam line ID15B. M. S.-C. would like to

thank CELTAM (Center for Low Temperature studies of Promising Materials for Applications) in Poland and the Academy of Finland for financing her research visit at the University of Helsinki. S.H., K.H. and S.M. were supported by the Academy of Finland (Contract No. 201291/40732). S.H. was supported also by the National Graduate School in Material Physics, which is funded by the Finnish Ministry of Education.

[1] M.J. Cooper, Rep. Prog. Phys. **48**, 415 (1985); S. Manninen, J. Phys. Chem. Solids **61**, 335 (2000).
[2] J. Radon, Ber. Verh. Sachs. AK MN **69**, 262 (1917).
[3] P.E. Mijnarends, Phys. Rev. **160**, 512 (1967).
[4] N.K. Hansen, HMI Report No. B342 (1980) (unpublished); N.K. Hansen, P. Pattison, and J.R. Schneider, Z. Phys. B: Condens. Matter **66**, 305 (1987).
[5] F.M. Mueller, Phys. Rev. B **15**, 3039 (1977); Y. Tanaka, N. Sakai, Y. Kubo, and H. Kawata, Phys. Rev. Lett. **70**, 1537 (1993).
[6] L. Dobrzyński and A. Holas, Nucl. Instrum. Methods Phys. Res. A **383**, 589 (1996).
[7] G. Reiter and R. Silver, Phys. Rev. Lett. **54**, 1047 (1985).
[8] G. Kontrym-Sznajd and M. Samsel-Czekała, Appl. Phys. A: Mater. Sci. Process. **70**, 89 (2000).
[9] G. Kontrym-Sznajd, R.N. West, and S.B. Dugdale, Mater. Sci. Forum **255-257**, 796 (1997); G. Kontrym-Sznajd, *First International Workshop on High Resolution Compton Scattering as a Probe of Fermiology, Kraków, Poland, 1993* (unpublished).
[10] D.G. Lock, V.H.C. Crisp, and R.N. West, J. Phys. F: Met. Phys. **3**, 561 (1973).
[11] A.M. Cormack, J. Appl. Phys. **34**, 2722 (1963); **35**, 2908 (1964); G. Kontrym-Sznajd, Phys. Status Solidi A **117**, 227 (1990).
[12] S. Huotari, K. Hämäläinen, S. Manninen, S. Kaprzyk, A. Bansil, W. Caliebe, T. Buslaps, V. Honkimäki, and P. Suortti, Phys. Rev. B **62**, 7956 (2000).
[13] K. Hämäläinen, S. Manninen, C.-C. Kao, W. Caliebe, J.B. Hastings, A. Bansil, S. Kaprzyk, and P.M. Platzman, Phys. Rev. B **54**, 5453 (1996).
[14] T.L. Loucks and P.H. Cutler, Phys. Rev. **133**, A819 (1964).
[15] B.R. Watts, Phys. Lett. **3**, 284 (1963).
[16] S. Chatterjee and P. Sinha, J. Phys. F: Met. Phys. **5**, 2089 (1975).
[17] D.A. Papaconstantopoulos, *Handbook of the Band Structure of Elemental Solids* (Plenum, New York, 1986), p. 54.
[18] B. Soulé de Bas, H.E. Dorsett, and M.J. Ford, J. Phys. Chem. Solids **64**, 495 (2003).
[19] L. Lam and P.M. Platzman, Phys. Rev. B **9**, 5122 (1974).
[20] S. Huotari, K. Hämäläinen, S. Manninen, C. Sternemann, A. Kaprolat, W. Schülke, and T. Buslaps, Phys. Rev. B **66**, 085104 (2002).
[21] A. Jura, G. Kontrym-Sznajd, and M. Samsel-Czekała, J. Phys. Chem. Solids **62**, 2241 (2001).
[22] M. Samsel-Czekała, G. Kontrym-Sznajd, G. Döring, W. Schülke, J. Kwiatkowska, F. Maniawski, S. Kaprzyk, and A. Bansil, Appl. Phys. A: Mater. Sci. Process. **76**, 87 (2003).
[23] J.H. Kaiser, R.N. West, and N. Shiotani, J. Phys. F: Met. Phys. **16**, 1307 (1986).
[24] Å. Björck and G. Dahlquist, *Numerical Methods* (Prentice-Hall, Englewood Cliffs, New Jersey, 1974).